

SUPERCONDUCTIVITY

Nearly ferromagnetic spin-triplet superconductivity

Sheng Ran^{1,2*}, Chris Eckberg², Qing-Ping Ding³, Yuji Furukawa³, Tristin Metz², Shanta R. Saha^{1,2}, I-Lin Liu^{1,2,4}, Mark Zic², Hyunsoo Kim², Johnpierre Paglione^{1,2}, Nicholas P. Butch^{1,2*}

Spin-triplet superconductors potentially host topological excitations that are of interest for quantum information processing. We report the discovery of spin-triplet superconductivity in UTe₂, featuring a transition temperature of 1.6 kelvin and a very large and anisotropic upper critical field exceeding 40 teslas. This superconducting phase stability suggests that UTe₂ is related to ferromagnetic superconductors such as UGe₂, URhGe, and UCoGe. However, the lack of magnetic order and the observation of quantum critical scaling place UTe₂ at the paramagnetic end of this ferromagnetic superconductor series. A large intrinsic zero-temperature reservoir of ungapped fermions indicates a highly unconventional type of superconducting pairing.

Topological superconductivity has attracted great interest in condensed matter physics because of its potential application for topological quantum computing (1–4). A promising platform for topological superconductivity and Majorana fermions is the spin-triplet superconducting pairing state. For instance, the earliest theoretical model system of topological superconductivity was a one-dimensional (1D) spinless p-wave superconductor, which hosts Majorana zero modes at the ends of the chain (5). In 2D spinless chiral p-wave superconductors, Majorana zero modes bind to the superconducting vortices (6). However, triplet pairing rarely exists in nature—only a dozen from the few thousand superconducting compounds discovered so far have been identified as candidate materials. Therefore, in the past decade, the experimental realization of topological superconductors has been sought in engineered topological phases, such as heterostructures in which triplet pairing is induced by proximity effect with conventional s-wave superconductors (7). Intrinsic triplet superconductors, where the pairing state emerges by virtue of the materials' internal properties, have been underexplored owing to the limited number of candidate compounds, such as Sr₂RuO₄ (8–10) and UPt₃ (11, 12).

Here, we report the discovery of a flavor of superconductivity in UTe₂ that exhibits the crucial ingredients of a spin-triplet pairing state—namely, an extremely large, anisotropic upper critical field H_{c2} ; temperature-independent nuclear magnetic resonance (NMR) Knight shift; and power law behavior of electronic specific heat and

nuclear spin-lattice relaxation rate in the superconducting state. In addition, UTe₂ closely resembles ferromagnetic superconductors, but with a dramatically enhanced transition temperature and upper critical field relative to known compounds (13–16), and a paramagnetic normal state; this suggests that UTe₂ is the paramagnetic end member of a ferromagnetic superconductor series.

UTe₂ crystallizes in the orthorhombic, centrosymmetric structure (space group *71 Immm*). U atoms compose parallel linear chains oriented along the [100] *a* axis (Fig. 1C), which coincides with the magnetic easy axis, as seen in the magnetic susceptibility M/H , where M is magnetization and H is magnetic field strength (Fig. 2A). The low symmetry of this structure is responsible for the large magnetic anisotropy (17), similar to the anisotropy in the orthorhombic, ferromagnetic superconductors URhGe and UCoGe (14, 15). Unlike these compounds, or the isoelectronic compound USe₂ (18), the temperature dependence of the magnetization and electrical resistivity show no indications of a phase transition to a magnetically ordered state (Fig. 2). The high-temperature magnetization data show paramagnetic behavior along all three crystallographic axes. A Curie-Weiss fit yields an effective moment of 2.8 bohr magnetons per unit (μ_B/U), reduced from the value of a fully degenerate $5f^2$ or $5f^3$ configuration. At low temperatures, the magnetization decreases along the *b* axis and becomes temperature-independent, a signature of Kondo coherence (19), whereas along the *a* axis the magnetization increases sharply and then shows a slight slope change at ~10 K, likely thanks to the Kondo coherence as well. No indication of phase transition at 10 K is observed from specific heat (see fig. S10) or resistivity measurements (Fig. 2C).

The high-temperature electrical resistivity $\rho(T)$ is typical of uncorrelated, paramagnetic moments in the presence of single-ion Kondo hybridization with the conduction band, which is respon-

sible for the negative slope. At temperatures below a crossover marked by maximal resistivity, the Kondo hybridization yields coherent electronic bands, resulting in a metallic temperature-dependence (Fig. 2C). Although UTe₂ does not magnetically order, the low-temperature magnetic behavior shows that UTe₂ is on the verge of ferromagnetism. Below 10 K, the *a* axis magnetization exhibits neither conventional field/temperature (H/T) paramagnetic scaling nor Arrott-Noakes ferromagnetic critical scaling (20) (see fig. S7). Instead, the data scale in accordance with the Belitz-Kirkpatrick-Vojta (BKV) theory of metallic ferromagnetic quantum criticality (21). For temperatures < 9 K and fields < 3 T, the magnetization data scale as M/T^β versus $H/T^{\beta+\gamma}$ (Fig. 2D), using BKV critical exponents ($\beta = 1$, $\gamma = 0.5$, $\delta = 1.5$), behavior that has only otherwise been observed in NiCoCr_{0.8} (22). This scaling, extending over five orders of magnitude, indicates that UTe₂ is a quantum critical ferromagnet, dominated by strong magnetic fluctuations. BKV theory applies to disordered metals and therefore, in principle, should not be applicable to UTe₂, which is in the clean limit (with a residual resistivity ratio of ~30). Instead, a ferromagnetic quantum phase transition is expected to be first order in the clean limit (23). Therefore, the observation of quantum criticality in UTe₂ calls for a different theory.

The transition from this correlated normal state to a superconducting ground state below the critical temperature $T_c = 1.6$ K is robust and sharp, as is evident in the low-temperature $\rho(T)$, ac magnetization $\chi(T)$ and specific heat $C(T)$ data (Fig. 3). There is a large residual value of the Sommerfeld coefficient $\gamma_0 = 55$ mJ/mol·K² in the superconducting state, or approximately half of the normal state value 110 mJ/mol·K², from which it is immediately apparent that either a large fraction of the sample is not superconducting or half of the conduction electrons at the chemical potential in this material are not gapped by the superconducting transition; the latter is indicative of an unconventional pairing mechanism, such as what occurs in UPt₃, UCoGe, and UGe₂ (24, 25). There is little variation in the residual γ_0 value between samples of UTe₂ with slightly different T_c (fig. S12), suggesting that the large residual electronic density of states is likely an intrinsic, disorder-insensitive property of UTe₂. The normalized jump in $C(T)$ at T_c is $\Delta C/\gamma T_c = 2.5$, which is much larger than the conventional Bardeen-Cooper-Schrieffer value of 1.43 expected from weak coupling, placing the system in the strong coupling regime; here, γ includes only the part that superconducts below T_c and is obtained by subtracting the residual value from the full value. For temperatures below T_c , $C(T)$ follows a power law, with the exponent $n \sim 3.2$, reflecting the presence of point nodes.

Perhaps the most pronounced sign of unconventional superconductivity is obvious in the upper critical field H_{c2} of this superconductor. The resistivity as a function of temperature for different magnetic fields applied along the three principal crystal axes is shown in Fig. 4. The H_{c2}

¹NIST Center for Neutron Research, National Institute of Standards and Technology, Gaithersburg, MD 20899, USA.

²Department of Physics, Center for Nanophysics and Advanced Materials, University of Maryland, College Park, MD 20742, USA. ³Ames Laboratory, U.S. Department of Energy and Department of Physics and Astronomy, Iowa State University, Ames, IA 50011, USA. ⁴Department of Materials Science and Engineering, University of Maryland, College Park, MD 20742, USA.

*Corresponding author. Email: sran@umd.edu (S.R.); nbutch@umd.edu (N.P.B.)

is strongly anisotropic, with the value along b exceeding the two orthogonal directions by a factor of 4 at 1 K. The zero-temperature limit of H_{c2} along b well exceeds the highest measured magnetic field of 20 T, and we conservatively estimate a value of 40 T on the basis of the curvature of the critical field in UCoGe (26). The H_{c2} value is very sensitive to the alignment of magnetic field along the b axis (fig. S5).

The upper critical field of a conventional singlet superconductor is restricted by both of the orbital and paramagnetic pair-breaking effects. The zero-temperature orbital limit in superconductors is often well described by the Werthamer-Helfand-Hohenberg (WHH) theory $H_{orb} = 0.7 dH_{c2}/dT_c|_{T_c} T_c$ (27). Although it can account for the response to field along the a axis, the WHH model otherwise disagrees drastically with our experimental results, most prominently along the b axis, where the slope of H_{c2} at T_c is ~ 17 T/K along b , which leads to an expected $H_{orb} = 20$ T for this direction. The conventional paramagnetic zero-temperature limit is given by $H_{para} = 1.86 T_c$ (28), yielding $H_{para} = 3$ T for UTe_2 . In the zero-temperature limit, the experimental H_{c2} value well exceeds H_{para} in all three directions and by almost an order of magnitude along the b axis, excluding spin-singlet order parameters.

The violation of the orbital limit in directions perpendicular to the magnetic easy axis (the a axis) is consistent with the behavior of the ferromagnetic superconductors (29) and differs qualitatively from the relatively low H_{c2} values found in other paramagnetic triplet superconductors (8, 30). The unusual shape of the H_{c2} curve of UTe_2 resembles those of UCoGe (26) and URhGe (31), in which ferromagnetic spin fluctuations are believed to mediate the superconducting pairs (25). Although the normal state of UTe_2 is not magnetically ordered, the notable similarities suggest that its superconducting pairs are also mediated by ferromagnetic spin fluctuations, indicating that it is the end member of the series of ferromagnetic superconductors. When superconducting pairing is mediated by ferromagnetic spin fluctuations, the field dependence of the magnetization is coupled to the field dependence of the superconducting coupling strength (32), as verified in UCoGe and URhGe (33). The coupling strength λ as a function of magnetic field can be estimated based on the behavior of H_{c2} and γ (24). Especially prominent is the large increase in λ along the b axis of $\sim 50\%$ (fig. S6), which far exceeds the field-induced enhancement of λ in UCoGe (33).

Further confirmation of spin-triplet pairing in UTe_2 comes from NMR measurements, which are sensitive to internal magnetic fields (Fig. 3D). No change of the peak position is observed in the ^{125}Te -NMR spectra between normal and superconducting states, leading to a temperature-independent value of the ^{125}Te Knight shift K , which is proportional to the spin susceptibility of the quasiparticles forming the superconducting pairs. In singlet-paired superconductors, K decreases below T_c , whereas in UTe_2 , K remains

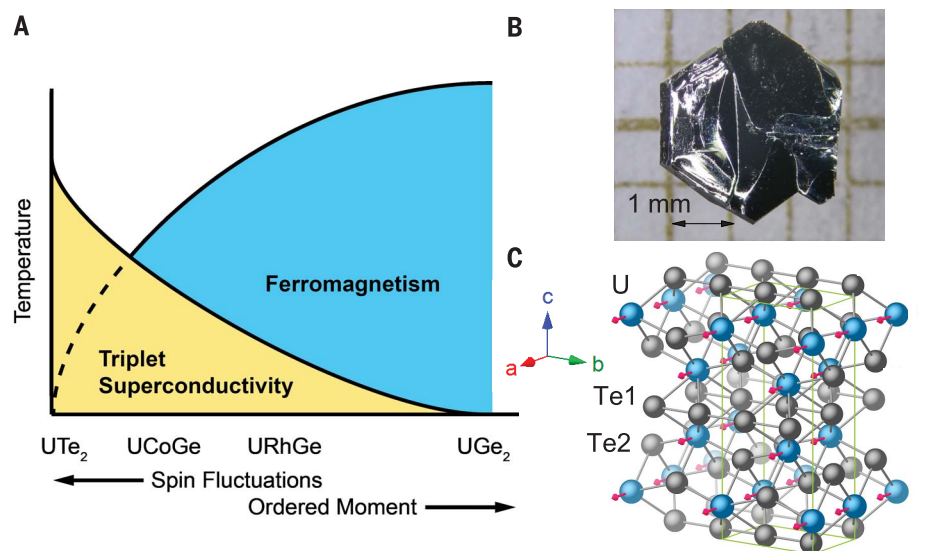


Fig. 1. Structure of UTe_2 . (A) Global phase diagram of ferromagnetic superconductors; UTe_2 is located at the paramagnetic end of the series. (B) A photo of a single crystal of UTe_2 grown using chemical vapor transport method on the millimeter scale. (C) Crystal structure of UTe_2 , with U atoms in blue and Te atoms in gray. The U atoms sit on chains parallel to the [100] a axis, which coincides with the magnetic easy axis, illustrated by the magenta arrows.

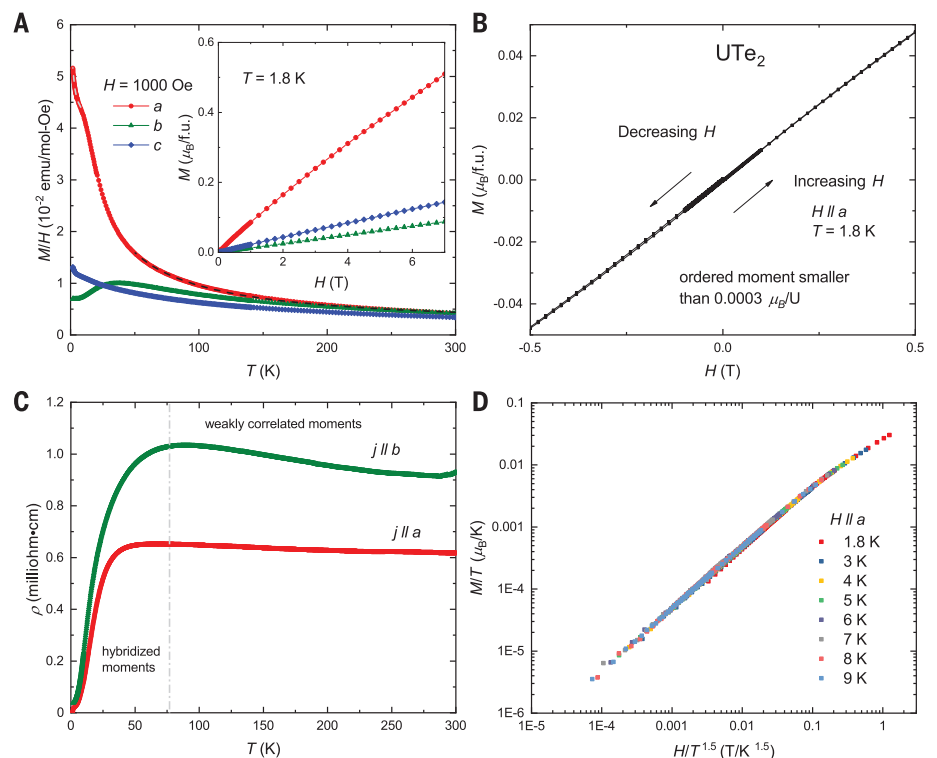


Fig. 2. Normal state properties of UTe_2 . (A) Temperature dependence of magnetization for three different directions of magnetic field of 0.1 T. For the field in a direction, the gray dashed line is the fit to the power law in the low-temperature region, whereas the black dashed line is the fit to the Curie-Weiss law in the high-temperature region. (Inset) Magnetization as a function of applied field in three directions at 1.8 K. (B) Magnetization data at 1.8 K upon increasing and decreasing magnetic field in the low field range showing no hysteresis. The upper bound for an ordered moment is $0.0003 \mu_B/U$ obtained from the zero field magnetization value. (C) Temperature dependence of electric resistivity data in zero magnetic field with electric current applied along a and b axes. (D) M/T as a function of $H/T^{1.5}$ for different temperatures. All the data collapse onto a single line. This scaling corresponds to the BKV theory of metallic ferromagnetic quantum criticality (see text).

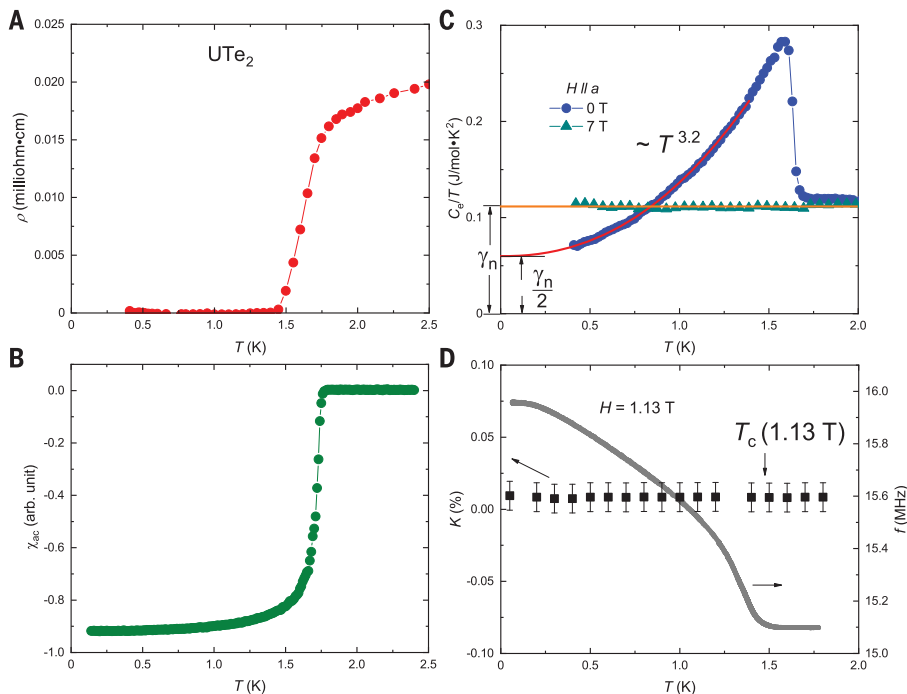


Fig. 3. Superconducting state properties of UTe₂. Temperature dependence of (A) resistivity and (B) ac magnetization data at low temperatures showing bulk superconductivity. (C) Electric contribution to heat capacity (phonon contribution has been subtracted as explained in the supplementary materials) in zero field and 7 T, divided by temperature, is shown as a function of temperature, illustrating γ in the superconducting and normal states. Magnetic field is applied along the *a* axis. (D) Temperature dependence of ¹²⁵Te NMR Knight shift *K* below and near *T_c* of powdered UTe₂ sample (left axis) and of the resonance frequency *f* of the NMR tank circuit confirming the superconducting state and *T_c* (right axis). *H* = 1.13 T.

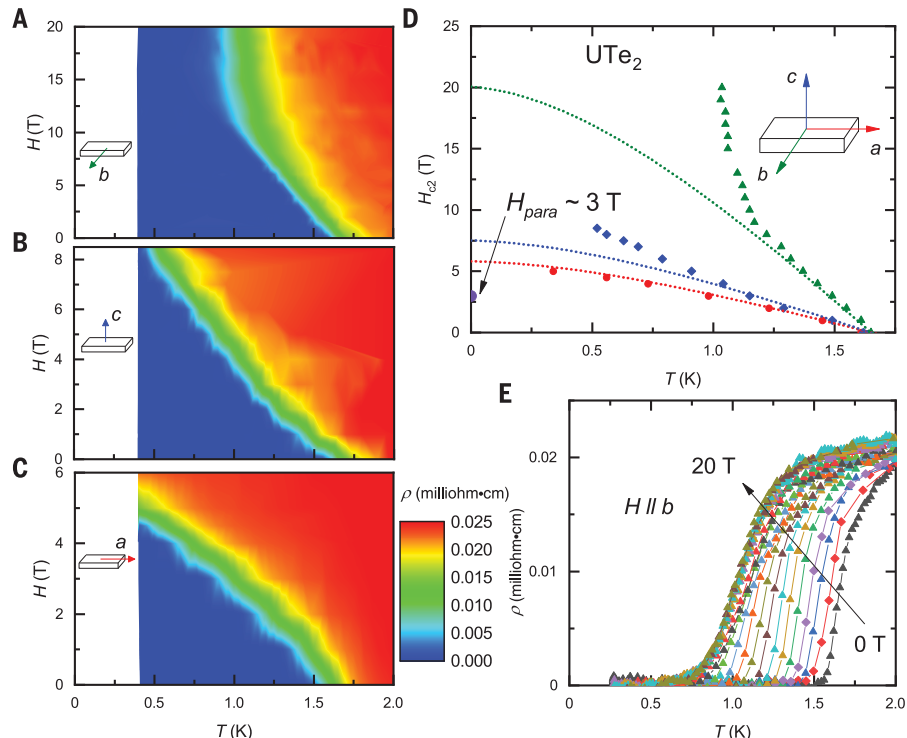


Fig. 4. Upper critical field *H_{c2}* of UTe₂. (A to C) Color contour plots of resistivity value as a function of temperature and magnetic field, with magnetic fields applied along (A) the *b* axis, (B) the *c* axis, and (C) the *a* axis. The current is applied along the *a* axis. (D) The *H_{c2}* value as a function of *T* in three directions. Dotted lines represent the WHH fit of the *H_{c2}* data. (E) Temperature-dependent resistivity data in magnetic fields applied along the *b* axis up to 20 T. Curves were measured using a constant magnetic field interval of 1 T.

constant on passing through *T_c*, signifying that the superconducting pair is a spin triplet (34, 35). The unconventional nature of the superconductivity in UTe₂ is also observed in the temperature dependence of ¹²⁵Te nuclear spin-lattice relaxation rate $1/T_1$ (fig. S16). $1/T_1$ shows a steep drop below ~ 1 K without showing a Hebel-Slichter coherence peak in $1/T_1$ just below *T_c*, which is expected for conventional BSC superconductors. The temperature dependence of $1/T_1$ below *T_c* follows a power law behavior $1/T_1 \sim T^6$ which is close to the $1/T_1 \sim T^5$ relation expected from the point-node gap structure (36, 37), consistent with the results of the specific heat measurement.

Having established clear evidence for spin-triplet pairing, one possible superconducting pairing symmetry consistent with a large fraction of ungapped electronic states of UTe₂ is the nonunitary triplet state, in which a two-component superconducting order parameter has two different energy gaps. However, such a state is generally not expected for paramagnetic, orthorhombic systems with strong spin-orbit coupling—this scenario applies to UTe₂ unless the effective spin-orbit coupling is demonstrated to be weak owing to special circumstances. No other standard archetype fits all measured properties of UTe₂, and any candidate state must account for the large field anisotropy, nodal gap structure, and the large residual electronic density of states, which are by themselves unusual. The high upper critical field itself suggests that the superconducting state resembles a condensate of equal spin pairs. One general possibility is band-selective superconductivity in a highly anisotropic electronic structure having multiple Fermi surfaces. Ongoing electronic structure measurements will help to determine whether such a description is applicable here. Regardless, explaining the relevance of ferromagnetic quantum criticality and the role of spin fluctuations will require further theoretical work.

The discovery of this superconducting state opens the door to advances in the study of spin-triplet pairing, topological electronic states, and their application to quantum information technology. As a paramagnetic version of ferromagnetic superconductors, UTe₂ is a promising topological superconductor (38) and may host Majorana excitations that can be detected by angle-resolved photoemission spectroscopy or scanning tunneling microscope (39).

REFERENCES AND NOTES

1. M. Sato, Y. Ando, *Rep. Prog. Phys.* **80**, 076501 (2017).
2. C. Beenakker, *Annu. Rev. Condens. Matter Phys.* **4**, 113–136 (2013).
3. S. D. Sarma, M. Freedman, C. Nayak, *npj Quantum Inf.* **1**, 15001 (2015).
4. J. Alicea, *Rep. Prog. Phys.* **75**, 076501 (2012).
5. A. Y. Kitaev, *Phys. Uspekhi* **44** (10S), 131–136 (2001).
6. N. Read, D. Green, *Phys. Rev. B* **61**, 10267–10297 (2000).
7. R. M. Lutchyn *et al.*, *Nat. Rev. Mater.* **3**, 52–68 (2018).
8. A. P. Mackenzie, Y. Maeno, *Rev. Mod. Phys.* **75**, 657–712 (2003).
9. C. Kallin, A. J. Berlinsky, *J. Phys. Condens. Matter* **21**, 164210 (2009).
10. Y. Maeno, S. Kittaka, T. Nomura, S. Yonezawa, K. Ishida, *J. Phys. Soc. Jpn.* **81**, 011009 (2012).
11. J. D. Strand *et al.*, *Science* **328**, 1368–1369 (2010).
12. E. R. Schermm, W. J. Gannon, C. M. Wishne, W. P. Halperin, A. Kapitulnik, *Science* **345**, 190–193 (2014).
13. S. S. Saxena *et al.*, *Nature* **406**, 587–592 (2000).

14. D. Aoki *et al.*, *Nature* **413**, 613–616 (2001).
15. N. T. Huy *et al.*, *Phys. Rev. Lett.* **99**, 067006 (2007).
16. D. Aoki, K. Ishida, J. Flouquet, *J. Phys. Soc. Jpn.* **88**, 022001 (2019).
17. S. Ikeda *et al.*, *J. Phys. Soc. Jpn.* **75** (suppl), 116–118 (2006).
18. H. Noël, M. Potel, R. Troc, L. Shlyk, *J. Solid State Chem.* **126**, 22–26 (1996).
19. G. R. Stewart, *Rev. Mod. Phys.* **56**, 755–787 (1984).
20. N. P. Butch, M. B. Maple, *Phys. Rev. Lett.* **103**, 076404 (2009).
21. T. R. Kirkpatrick, D. Belitz, *Phys. Rev. B* **91**, 214407 (2015).
22. B. C. Sales *et al.*, *npj Quantum Materials* **2**, 33 (2017).
23. M. Brando, D. Belitz, F. M. Grosche, T. R. Kirkpatrick, *Rev. Mod. Phys.* **88**, 025006 (2016).
24. R. Joynt, L. Taillefer, *Rev. Mod. Phys.* **74**, 235–294 (2002).
25. V. P. Mineev, *Phys. Uspekhi* **60**, 121–148 (2017).
26. D. Aoki *et al.*, *J. Phys. Soc. Jpn.* **78**, 113709 (2009).
27. E. Helfand, N. R. Werthamer, *Phys. Rev.* **147**, 288–294 (1966).
28. A. M. Clogston, *Phys. Rev. Lett.* **9**, 266–267 (1962).
29. V. P. Mineev, *Phys. Rev. B* **95**, 104501 (2017).
30. Z. F. Weng *et al.*, *Phys. Rev. Lett.* **117**, 027001 (2016).
31. F. Lévy, I. Sheikin, B. Grenier, A. D. Huxley, *Science* **309**, 1343–1346 (2005).
32. V. P. Mineev, *Phys. Rev. B* **83**, 064515 (2011).
33. B. Wu *et al.*, *Nat. Commun.* **8**, 14480 (2017).
34. H. Tou *et al.*, *Phys. Rev. Lett.* **77**, 1374–1377 (1996).
35. K. Ishida *et al.*, *Nature* **396**, 658–660 (1998).
36. J. Yang, Z. T. Tang, G. H. Cao, G. Q. Zheng, *Phys. Rev. Lett.* **115**, 147002 (2015).
37. K. Katayama *et al.*, *J. Phys. Soc. Jpn.* **76**, 023701 (2007).
38. A. K. C. Cheung, S. Raghu, *Phys. Rev. B* **93**, 134516 (2016).
39. J. D. Sau, S. Tewari, *Phys. Rev. B* **86**, 104509 (2012).
40. S. Ran, Replication data for: Nearly ferromagnetic spin-triplet superconductivity, Version 1, Harvard Dataverse (2019); <https://doi.org/10.7910/DVN/UJAFUC>.

ACKNOWLEDGMENTS

We thank W. Fuhrman, Y.-T. Hsu, T. Kong, S. Raghu, J. Sau, Y. Wang, S.-L. Xu, and V. Yakovenko for helpful discussions. We also thank H. Hodovanets for assistance during our experiments. **Funding:** Research at the University of Maryland was supported by the National Science Foundation Division of Materials Research Award DMR-1610349, U.S. Department of Energy (DOE) Award DE-SC-0019154, Air Force Office of Scientific Research Award FA9550-14-1-0332, and the Gordon and Betty Moore Foundations EPIQS Initiative through Grant GBMF4419. Research at Ames Laboratory was supported by the U.S. Department of

Energy (DOE), Office of Basic Energy Sciences, Division of Materials Sciences and Engineering. Ames Laboratory is operated for the U.S. DOE by Iowa State University under Contract DE-AC02-07CH11358. **Author contributions:** S.R. and N.P.B. conceived of and designed the study. S.R. and S.R.S. synthesized the single crystalline samples. S.R., C.E., I.-L.L., H.K., and J.P. performed the electrical resistivity measurements. S.R., C.E., and T.M. performed the specific heat measurements. S.R., S.R.S., and M.Z. performed the magnetization measurements. S.R. and N.P.B. performed the neutron scattering measurements. Q.-P.D. and Y.F. performed the NMR measurements. All authors contributed to the preparation of the manuscript. **Competing interests:** The authors declare no competing interests. **Data and materials availability:** Data are available at Harvard Dataverse (40).

SUPPLEMENTARY MATERIALS

science.sciencemag.org/content/365/6454/684/suppl/DC1
Materials and Methods
Supplementary Text
Figs. S1 to S16

29 October 2018; accepted 12 July 2019
10.1126/science.aav8645

Nearly ferromagnetic spin-triplet superconductivity

Sheng Ran, Chris Eckberg, Qing-Ping Ding, Yuji Furukawa, Tristin Metz, Shanta R. Saha, I-Lin Liu, Mark Zic, Hyunsoo Kim, Johnpierre Paglione and Nicholas P. Butch

Science **365** (6454), 684-687.
DOI: 10.1126/science.aav8645

An unusual superconductor

In conventional, and in many unconventional, superconductors, the electrons that form Cooper pairs have spins pointing in opposite directions. An applied magnetic field can easily "break" such pairs—and destroy superconductivity—by aligning both spins in the same direction. In contrast, spin-triplet superconductors are much more resilient to magnetic fields. Very few candidates for such materials have been discovered. Ran *et al.* add to this select group by observing signatures of spin-triplet superconductivity, including a very large and anisotropic upper critical magnetic field, in the material UTe₂. Because spin-triplet superconductors may naturally exhibit topological superconductivity, this material may also be of interest in quantum computing.

Science, this issue p. 684

ARTICLE TOOLS

<http://science.sciencemag.org/content/365/6454/684>

SUPPLEMENTARY MATERIALS

<http://science.sciencemag.org/content/suppl/2019/08/14/365.6454.684.DC1>

REFERENCES

This article cites 39 articles, 3 of which you can access for free
<http://science.sciencemag.org/content/365/6454/684#BIBL>

PERMISSIONS

<http://www.sciencemag.org/help/reprints-and-permissions>

Use of this article is subject to the [Terms of Service](#)



Supplementary Materials for

Nearly ferromagnetic spin-triplet superconductivity

Sheng Ran*, Chris Eckberg, Qing-Ping Ding, Yuji Furukawa, Tristin Metz,
Shanta R. Saha, I-Lin Liu, Mark Zic, Hyunsoo Kim, Johnpierre Paglione,
Nicholas P. Butch*

*Corresponding author. Email: sran@umd.edu (S.R.); nbutch@umd.edu (N.P.B.)

Published 16 August 2019, *Science* **365**, 684 (2019)
DOI: 10.1126/science.aav8645

This PDF file includes:

Materials and Methods
Supplementary Text
Figs. S1 to S16

Materials and Methods

Single crystals of UTe_2 were synthesized by the chemical vapor transport method using iodine as the transport agent. Elements of U and Te with atomic ratio 2:3 were sealed in an evacuated quartz tube, together with 3 mg/cm^3 iodine. The ampoule was gradually heated up and hold in the temperature gradient of $1060/1000 \text{ }^\circ\text{C}$ for 7 days, after which it was furnace cooled to room temperature. The crystal structure was determined by x -ray powder diffraction using a Rigaku x -ray diffractometer with Cu-K_α radiation. Crystal orientation was determined by Laue x -ray diffraction performed with a Photonic Science x -ray measurement system. Neutron scattering was performed on the NG-4 Disk Chopper Spectrometer at the NIST Center for Neutron Research.

Electrical resistivity measurements were performed in a Quantum Design Physical Property Measurement System (PPMS) using the ^3He option, and in Oxford ^3He system. Magnetization measurements were performed in a magnetic field of 0.1 T using a Quantum Design Magnetic Property Measurement System (MPMS). AC magnetic susceptibility measurements were performed in a Quantum Design PPMS using the ADR option. Specific heat measurements were also performed in a Quantum Design PPMS using the ^3He option, and in Oxford dilution refrigerator system.

Ultra-low temperature NMR measurements of ^{125}Te ($I = 1/2$, $\gamma_N/2\pi = 13.454 \text{ MHz/T}$) nuclei were conducted on powdered crystals using a lab-built phase coherent spin-echo pulse spectrometer and an Oxford dilution refrigerator installed at the Ames Lab. The ^{125}Te -NMR spectra were obtained by sweeping the magnetic field H at $f = 15.1 \text{ MHz}$. The data that support the results presented in this paper and other findings of this study are available from the corresponding authors upon reasonable request.

The ^{125}Te $1/T_1$ was measured in a magnetic field of 1.13 T with a recovery method using a single $\pi/2$ saturation pulse at the peak position of the spectrum. The $1/T_1$ at each T was determined by fitting the nuclear magnetization M versus time t using the exponential function $1 - M(t)/M(\infty) = e^{(-\frac{t}{T_1})^\beta}$, where $M(t)$ and $M(\infty)$ are the nuclear magnetization at time t after the saturation and the equilibrium nuclear magnetization at $t \rightarrow \infty$, respectively and β is the stretching exponent. Typical β values used are $0.3 \sim 0.5$. A fit with $\beta < 1$ indicates a distribution of relaxation rates, which mainly comes from the anisotropy in T_1 for different crystal directions in the powder sample in magnetic field.

Identification of commercial equipment does not imply recommendation or endorsement by NIST. Error bars correspond to an uncertainty of one standard deviation.

Supplementary Text

Part I. X-ray and neutron diffraction

Room temperature powder x-ray diffraction on crushed single crystals shows that CVT-grown UTe_2 forms in the correct crystal structure and is single phase, with no sign of impurity phases. Low-temperature neutron diffraction confirms that there are no structural or magnetic phase transitions down to 5 K.

Part II. Electrical resistivity

The low temperature resistivity can be fit to Fermi liquid term AT^2 (Fig. S4), with $A \sim 0.64 \mu\Omega\text{-cm/K}^2$ for a -axis and $1.55 \mu\Omega\text{-cm/K}^2$ for b -axis. Values of residual resistivity ratio (RRR) range from 18 to 30. These do not exhibit a large variation across different batches of single crystals synthesized via CVT.

The Kondo-coherent state exhibits strongly-renormalized Fermi liquid properties: 1) resistivity $\rho = AT^2$, with $A \sim 1 \mu\Omega\text{-cm/K}^2$, 2) specific heat $C = \gamma T$ with $\gamma = 120 \text{ mJ/mol-K}^2$, and 3) the Kadowaki - Woods ratio $A/\gamma^2 \sim 1 \times 10^{-4} \mu\Omega\text{-cm/K}^2/(\text{mJ/mol-K}^2)^2$, similar to many heavy fermion metals.

Part III. Magnetization

The Arrott plots (Fig. S6) in the low field range (0 - 0.1 T) at different temperatures show that the system is not in the critical regime of a mean-field classical (finite-temperature) ferromagnetic phase transition. Extending this analysis beyond mean field using the Arrott-Noakes equation of state is also unsuccessful.

The magnetization data can be well-described by M/T^β vs. $H/T^{\beta+\gamma}$ scaling. To determine critical exponents, the low temperature magnetization data was fitted to power law behavior, with $\gamma = 0.51$ (Fig. S7). There exists a constant susceptibility M/H , consistent with a large Pauli paramagnetic response from the heavy Fermi liquid. M/T^β vs. $H/T^{\beta+\gamma}$ data collapse onto a single curve, for temperatures less than 9 K and fields less than 7 T (Fig. S8), with the corresponding exponents $\beta = 4.16$, $\gamma = 0.51$, $\delta = 1.12$. The small value of δ reflects the almost-linear $M(H)$, but the very large value of β cannot be reconciled with any known theories. To conform to the established theory of metallic ferromagnetic critical behavior, Belitz-Kirkpatrick-Vojta (BKV) theory, the constant term in M/H , or equivalently a linear term in $M(H)$, is subtracted from the measured $M(H)$ data. After the subtraction, for temperatures less than 9 K and fields less than 3 T, the resultant curves also collapse onto a single curve when M/T^β is plotted vs. $H/T^{\beta+\gamma}$ (main text, Fig. 2), using BKV critical exponents ($\beta = 1$, $\gamma = 0.5$, $\delta = 1.5$). However, we note that BKV theory is constructed for disordered systems and therefore in principle should not be applicable for UTe_2 which is in the clean limit (with RRR about 30).

This may be the reason for ambiguity in the critical exponents, but certainly this case calls for theoretical attention.

Part IV. Specific heat

The low-temperature T^3 phonon contribution to the specific heat is estimated by fitting a linear function to C/T vs T^2 (Fig. S9). This contribution is subtracted from the specific heat data to obtain the electric contribution. It can also be seen that there are no signatures of magnetic phase transitions or unusual temperature-dependence above the superconducting T_c .

The deviation from BCS behavior of the superconducting transition in UTe_2 is emphasized in Fig. S10, in which it is clear that exponential temperature dependence expected for an isotropic gap is absent in this material. Instead, the specific heat below T_c follows a power law, with $n \sim 3.2$, reflecting the presence of point nodes, which arise from a momentum-dependent gap structure typical of nonunitary states.

The large residual γ is a robust feature and does not show obvious sample variation as seen in Fig. S11. This fact is in sharp contrast to the strong sample dependence observed in other materials considered to house spin-triplet superconductivity.

C/T data in the magnetic fields applied along a -axis are shown in Fig. S12. The residual γ increases systematically upon increasing magnetic field, further indicating this is an intrinsic property of the compound, as magnetic field will enhance spin unbalance. Entropy calculated from specific heat data for superconducting and normal state are shown in Fig. S13. The normal state data are obtained by applying a magnetic field of 7 T along the a -axis to suppress superconductivity. The superconducting jump releases 10% more entropy than expected, which can be ascribed to magnetic excitations arising from the spin-polarized ungapped normal Fermi liquid.

Part V. NMR

No change of the peak position has been observed in the ^{125}Te -NMR spectra between normal and superconducting states, as shown in Fig. S14. ^{125}Te nuclear spin-lattice relaxation rate $1/T_1$, presented in Fig. S15, shows a steep drop below about 1 K without showing a Hebel-Slichter coherence peak in $1/T_1$ just below T_c which is expected for conventional BSC superconductors. The temperature dependence of $1/T_1$ below T_c follows a power law behavior $1/T_1 \sim T^6$ which is close to the $1/T_1 \sim T^5$ relation expected from the point-node gap structure, consistent with the results of specific heat measurements.

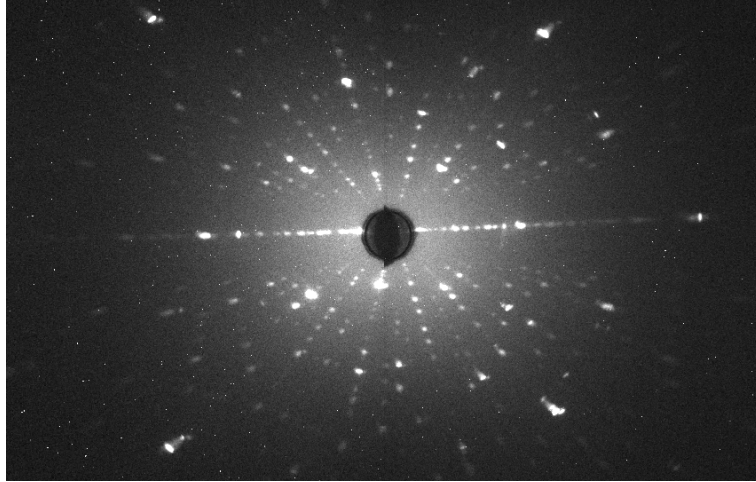


Figure S1: Laue diffraction pattern of [011] direction demonstrating good crystallinity.

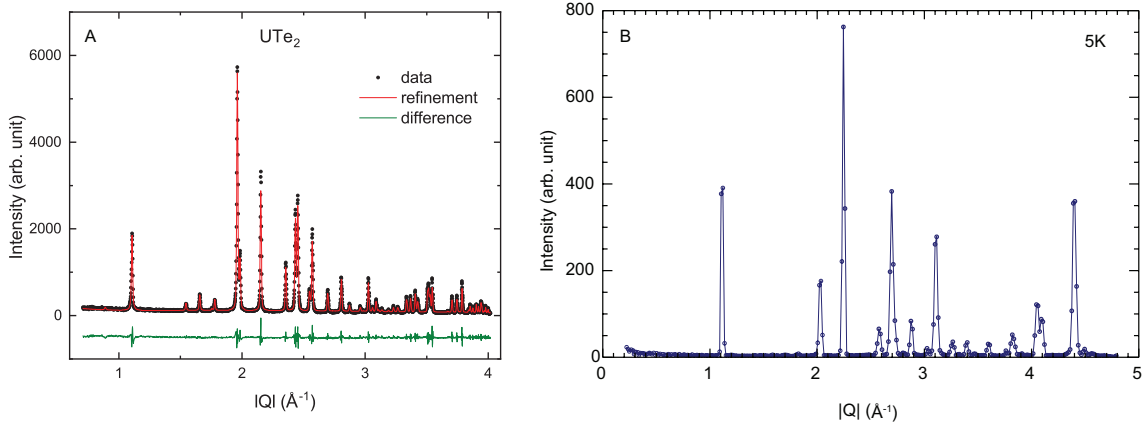


Figure S2: **Powder x-ray and neutron diffraction data of UTe_2 .** (A) Powder *x*-ray diffraction data of UTe_2 showing good quality of the sample with no visible peaks from impurities. (B) Low-temperature neutron diffraction data of UTe_2 confirming that there are no structural or magnetic phase transitions down to 5 K.

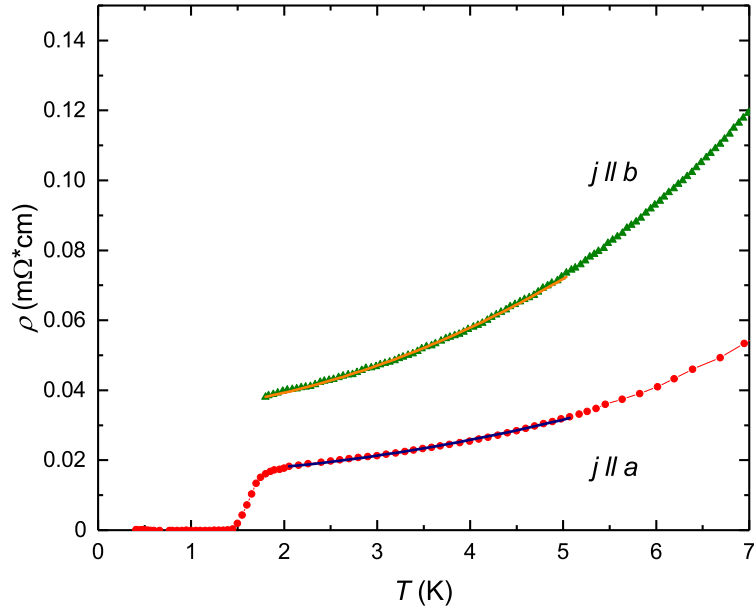


Figure S3: **Temperature dependence of electrical resistivity data in zero magnetic field.** Electric current is applied along *a* and *b*-axis. The lines are the fit to Fermi liquid formula AT^2 .

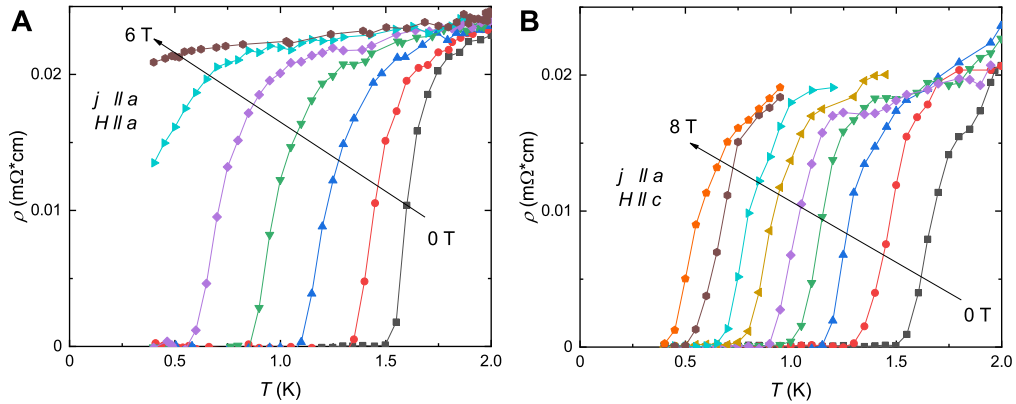


Figure S4: **Temperature dependent resistivity data in magnetic fields.** Magnetic fields are applied along (A) *a* and (B) *c* axis. The current is applied along *a*-axis. Curves were measured using a constant magnetic field interval of 1 T.

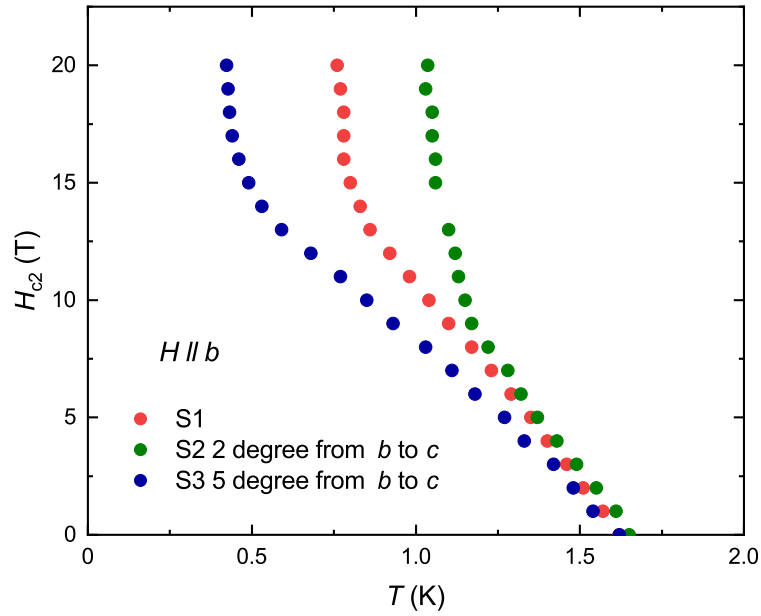


Figure S5: **Upper critical field H_{c2} as a function of T for magnetic field along b -axis for three samples of UTe_2 .** S2 and S3 are orientated about 2 and 5 degrees from b towards c axis.

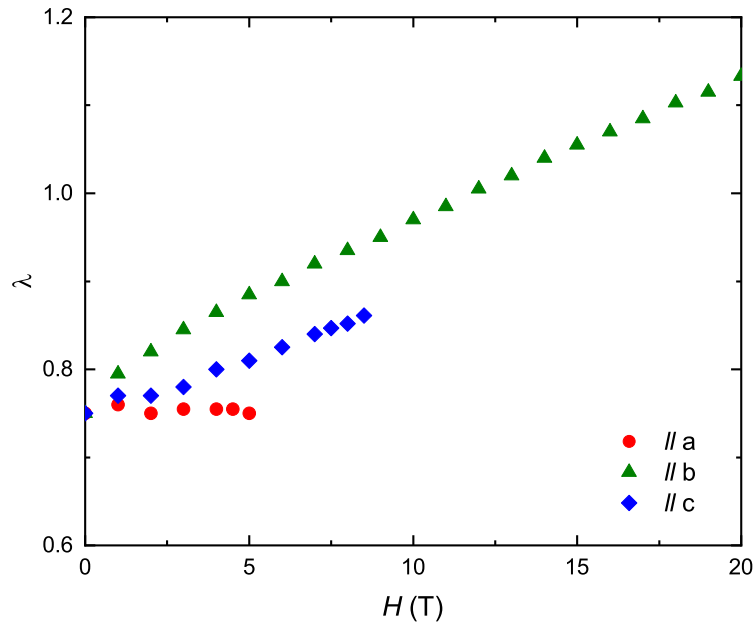


Figure S6: **Coupling strength of UTe_2 .** The calculated superconducting coupling strength as a function of applied magnetic field in three directions is enhanced when field is applied along the b -axis, as expected from pairing due to ferromagnetic fluctuations.

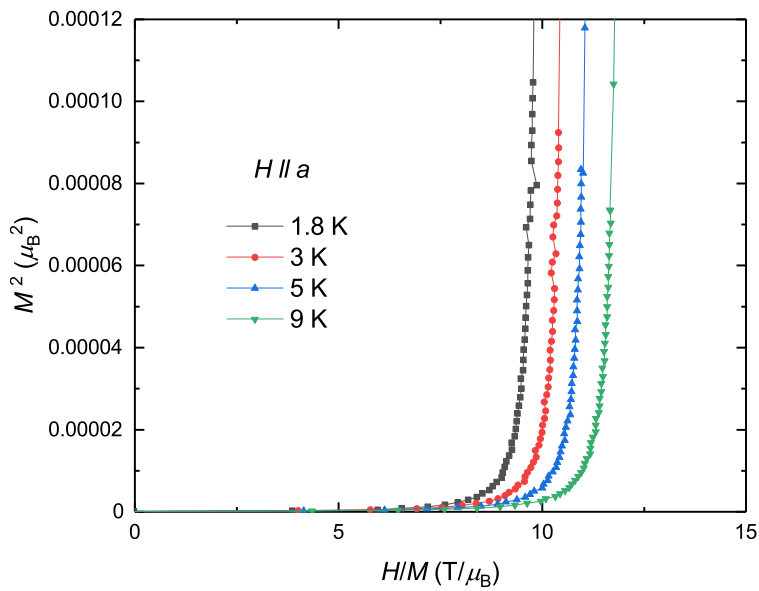


Figure S7: **Arrott plot, M^2 as a function of H/M , at different temperatures above T_c .** It can be seen that UTe_2 does not have a conventional finite-temperature ferromagnetic transition.

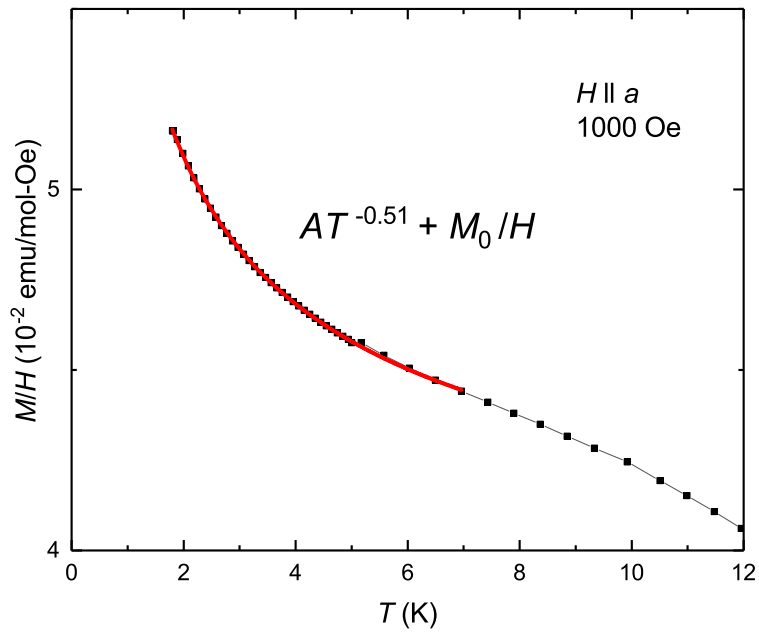


Figure S8: **Temperature dependence of magnetization.** Magnetic field of 0.1 T is applied along a axis. The red line is the fit to the power law $AT^v + M_0/H$ in the low temperature region. The constant term M_0 is necessary to obtain a good fitting.

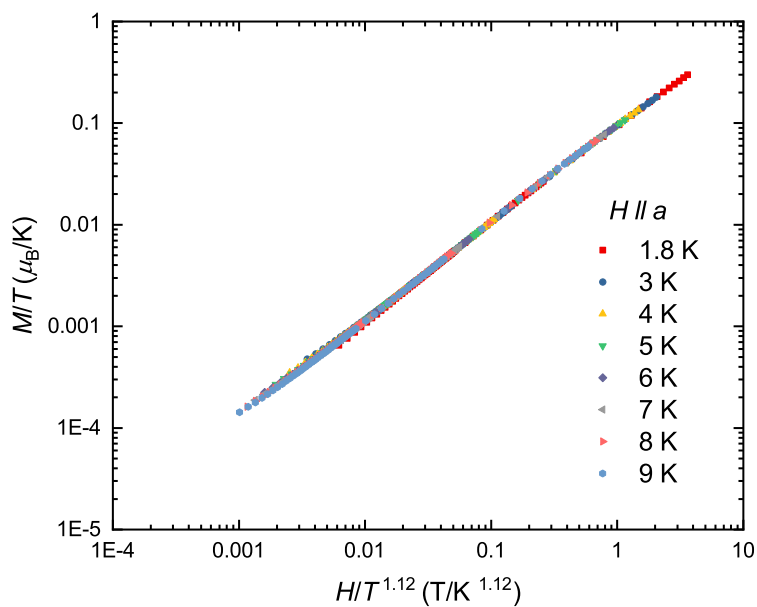


Figure S9: M/H as a function of $H/T^{1.12}$ for different temperatures. All the data collapse onto a single line.

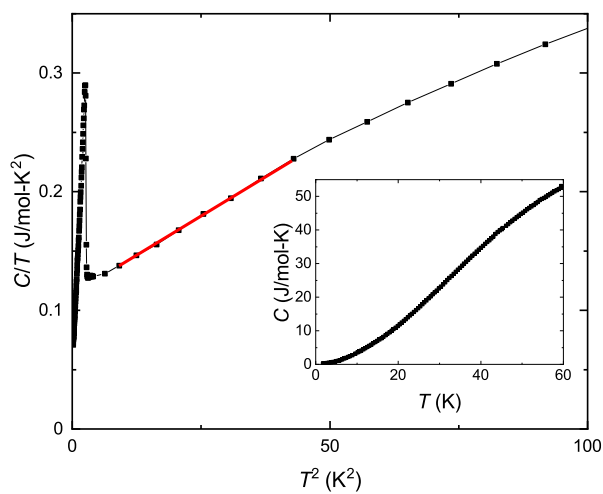


Figure S10: C/T data as function of T^2 . There is a linear region above T_c , from which a phonon contribution to the specific heat is obtained by fitting to a linear function. The red line is the fit. Inset: C as function of T . No magnetic order is detected above T_c .

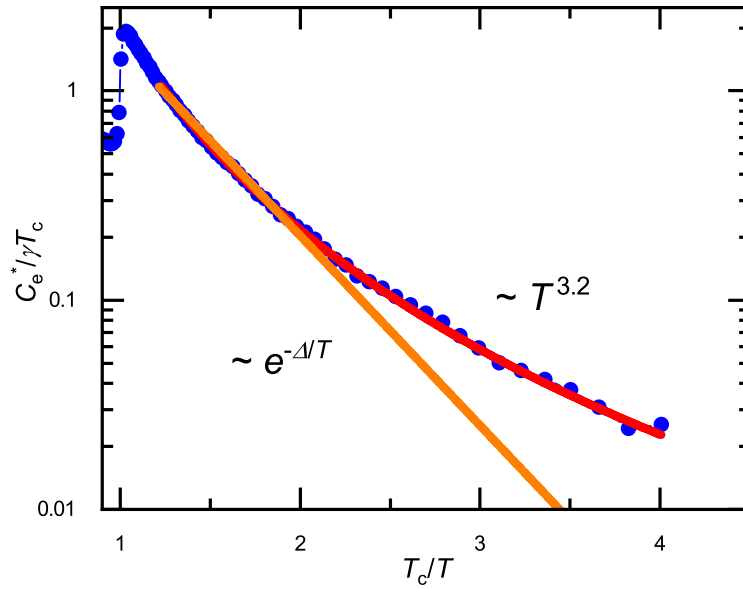


Figure S11: **Semilog plot of $C_e^*/\gamma T_c$ as a function of T_c/T .** C_e^* is the electric contribution to specific heat minus the residue term at the zero temperature limit. Orange line is the fit to the BCS fully gapped function and it does not describe the data well at low temperatures. Red line is the fit to a power law with $n = 3.2 \pm 0.1$.

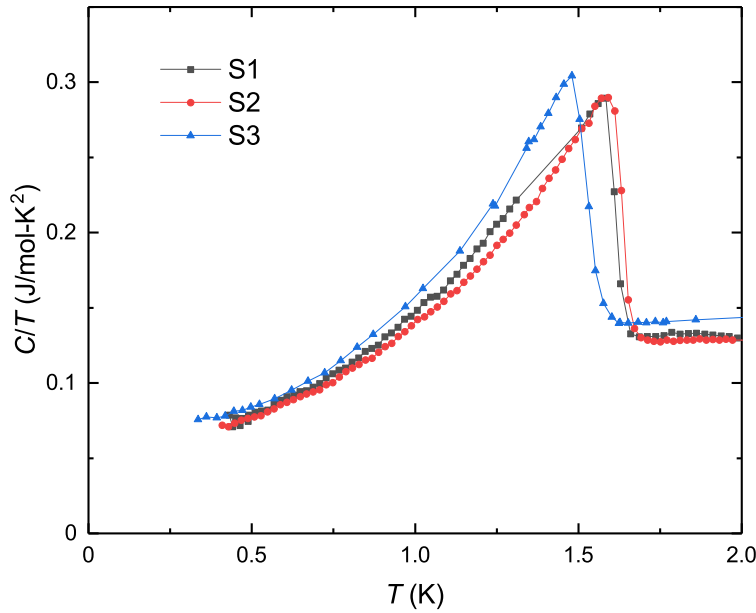


Figure S12: **C/T data for different samples.** The residual γ in the superconducting state does not show obvious sample variation.

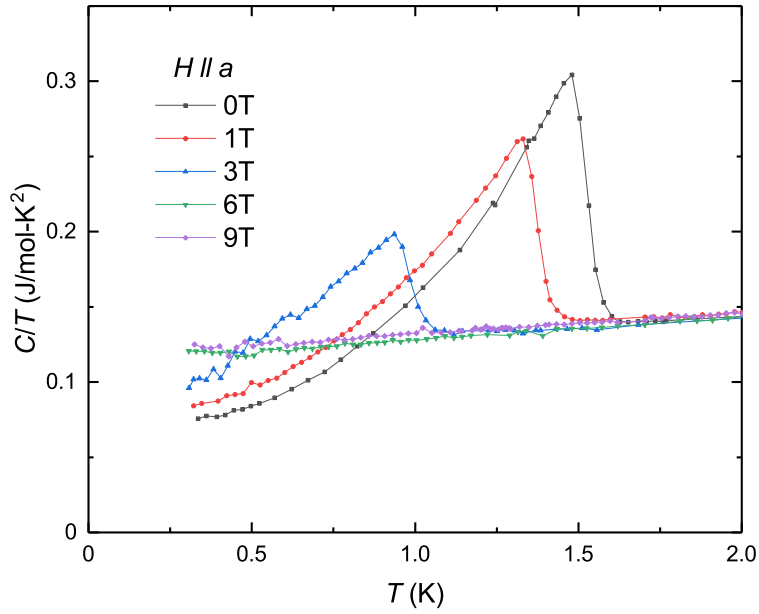


Figure S13: **C/T data in different magnetic fields.** Magnetic fields are applied along a -axis. H_{c2} is approximately 6 T in this direction. The large normal state C/T is that of a heavy Fermi liquid.

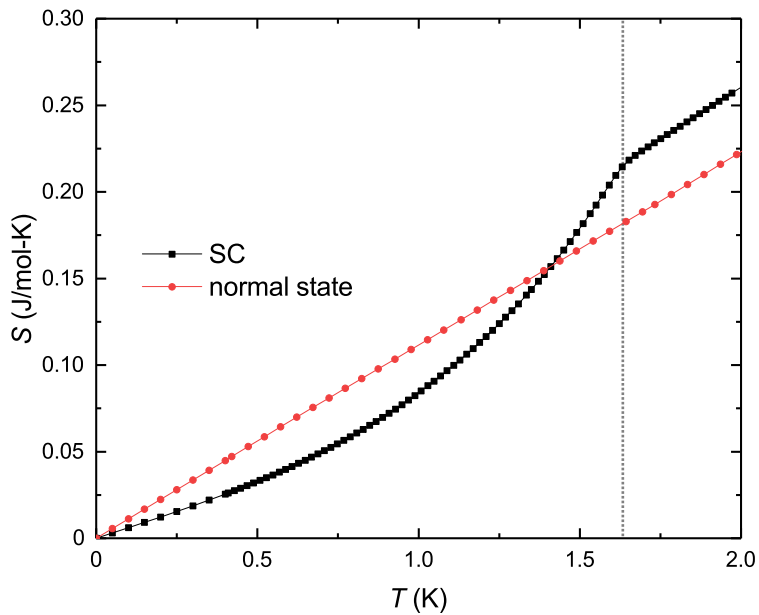


Figure S14: **Entropy calculated from specific heat data for superconducting and normal states.** The normal state data are obtained by applying magnetic field of 7 T along the a -axis to suppress superconductivity.

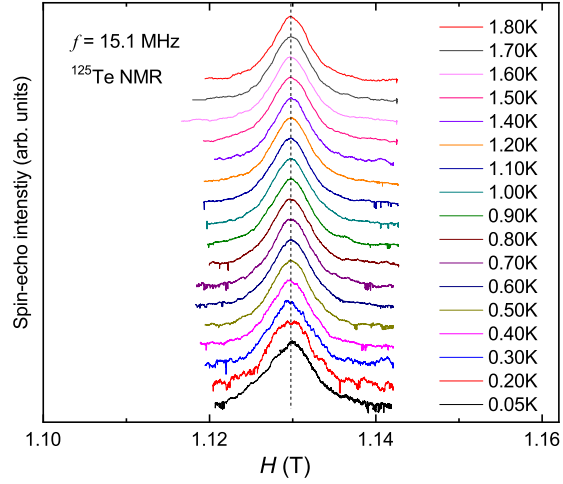


Figure S15: ^{125}Te NMR spectra in both the normal and the superconducting states of UTe_2 at $f = 15.1$ MHz.

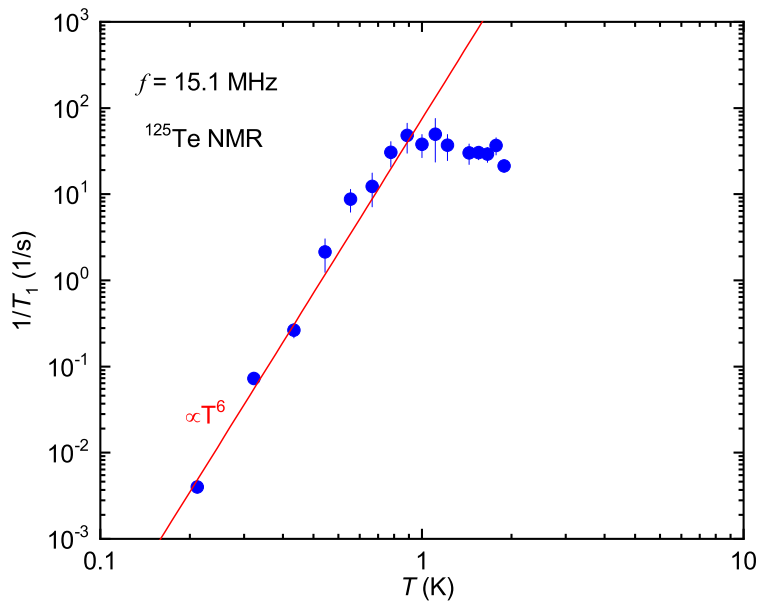


Figure S16: Temperature dependence of ^{125}Te nuclear spin-lattice relaxation rate $1/T_1$ of UTe_2 in magnetic field of 1.13 T. The red line is the fit to the power law in the low temperature region.